Composites Part A 111 (2018) 62–72

Contents lists available at ScienceDirect

Composites Part A

journal homepage: www.elsevier.com/locate/compositesa

Reduced notch sensitivity in pseudo-ductile CFRP thin ply angle-ply laminates with central 0° plies

Xun Wu*, Jonathan D. Fuller, Marco L. Longana, Michael R. Wisnom

Bristol Composites Institute (ACCIS), University of Bristol, Bristol BS8 1TR, United Kingdom

ARTICLE INFO

Keywords:
B. Fragmentation
B. Delamination
B. Stress concentrations
C. Damage mechanics

ABSTRACT

This paper presents an experimental investigation on the unnotched and open-hole tensile behaviour of pseudo-ductile thin ply angle-ply carbon fibre/epoxy laminates with central 0° plies. Laminates with two different configurations of $[\pm 26_5/0]_s$ and $[\pm 25_2/0]_s$ were designed and tested under unnotched and open-hole tensile loading. Metal-like tensile stress-strain curves with a plateau were observed in both unnotched configurations. The open-hole net-section strength of the $[\pm 25_2/0]_s$ laminate attained 96% of the unnotched "yield" strength. Digital image correlation and X-ray CT-scan images showed that the same damage mechanisms of central 0° ply fragmentation and local dispersed delamination observed in unnotched pseudo-ductile laminates were present in the open-hole specimens of the same configuration. These damage mechanisms caused stress redistribution around the hole and reduced the notch sensitivity in pseudo-ductile laminates under open-hole tensile loading. The main factors governing the open-hole performance are also discussed.

1. Introduction

One of the main limitations of high performance carbon fibre reinforced polymer composites (CFRP) is that they can fail catastrophically without any warning, so a greater safety margin needs to be considered when designing a structure from CFRP. Therefore, achieving "ductility" in carbon fibre composites is crucial and up to now, a number of different approaches have been developed, such as introducing ductile constituents [1–4] or by re-designing the architectures of carbon fibre laminates, for example using the extra strain generated by fibre reorientation [5–8] and making hybrid composites via either interlayer/ply-by-ply hybrids [9–12] or intermingled hybrids [13,14].

By using the fibre reorientation approach, Fuller et al. [7] showed that gradual failure can be achieved in a thin ply angle-ply laminate with central 0° plies. A high ultimate tensile strength and strain to failure have been found in $[\pm \theta_n]_s$ laminates using thin ply prepreg [5,6]. Subsequently, an analytical model was developed to predict the behaviour of $[\pm \theta_n/0_m]_s$ laminates, by incorporating the non-linear behaviour of angle plies and several possible failure modes such as 0° ply fragmentation, Mode II dispersed delamination at the $-\theta/0$ interface and fracture of the angle plies [7]. The predictions were then validated by experiment. A metal-like pseudo-ductile tensile stress-strain behaviour was experimentally demonstrated for a $[\pm 26_5/0]_s$ laminate with Skyflex USN020 prepreg (with fibre type TR30 and nominal ply thickness t = 0.03 mm) for all plies and the results showed a good agreement with the analytical model. A considerable strain to failure of 4.2% with a "yield" stress of 692 MPa was attained.

Pseudo-ductility and unique damage mechanisms have been found in these thin ply angle-ply laminates in tension. However, to progress these laminates towards real applications, their open-hole behaviour needs to be understood since the presence of stress concentrations can lead to catastrophic failure and significant strength reduction.

In previous research, notch sensitivity has been found to be related to the damage within the laminate prior to the final failure. In order to understand the relation between damage and notched strength, Kortschot and Beaumont [15] conducted a series of tensile tests on notched cross-ply laminates and employed an X-ray machine to monitor damage in the specimen. They concluded that the sub-critical damage in cross-ply laminates, such as 0° ply splitting, transverse ply cracking and delamination, can redistribute the stress and have a significant influence on the notched strength of the laminate.

The effect of sub-critical damage on notched strength has also been discussed in studies of laminate thickness and scaling effects in notched composites. Harris and Morris [16] tested a number of quasi-isotropic (QI) laminates with different numbers of sub-laminates in order to study the role of delamination and damage on notched strength. They found that the notched strength was reduced in thicker laminates, since delamination growth was limited in the through thickness direction. Green et al. [17] carried out a series of open-hole tensile tests with

* Corresponding author.
E-mail address: xunxun.wu@bristol.ac.uk (X. Wu).

https://doi.org/10.1016/j.compositesa.2018.05.011
Received 14 July 2017; Received in revised form 9 May 2018; Accepted 11 May 2018
Available online 25 May 2018

different hole diameters and ply thicknesses to investigate the scaling effects in notched composites. The results showed the trend that having less sub-critical damage in a laminate with less ply blocking, resulted in a larger strength reduction. This is due to the fact that sub-critical damage can redistribute the stress around the hole and delay the onset of final failure.

From the studies mentioned above, it is clear that the notch-sensitivity of a laminate is highly related to the damage development within the laminate prior to final fracture. Subcritical damage can redistribute the stress concentration at the notch-tip and therefore achieve a higher notched strength. However, this could be a concern with laminates using thin plies, since the damage suppression characteristic in thin plies has been shown to be sensitive to notches [18–21]. In all of these studies, the unnotched tensile strength increased considerably with a reduction in ply thickness, but the open-hole tensile strength can be at least 10% lower than the thicker one, whilst failing in a more brittle manner.

In order to improve the notched performance of thin-ply laminates and maintain the benefits of using thin ply prepreg, it is necessary to design the laminate with "built in" damage. Furtado et al. [19] developed a selective ply-level hybridisation concept, which combined off-axis thin plies with standard thickness 0° plies in a QI laminate. The splitting of the 0° plies was the main mechanism for reducing notch sensitivity and the thin off-axis plies delayed or suppressed further delamination within the gauge section. Jalalvand et al. [22] also suggested based on numerical modelling, that the notch sensitivity can be reduced in QI laminates made from pseudo-ductile thin-ply hybrid sub-laminates. The results showed that when the ratio of pseudo-ductile strain to "yield" strain is sufficiently high, the stress concentration can be reduced since damage of the pseudo-ductile thin-ply hybrid sub-laminate initiated and re-distributed the stress around the hole.

The aim of this paper is to investigate the open-hole tensile performance of pseudo-ductile thin ply angle-ply laminates based on a single hole size, to understand the role of the damage mechanisms of these pseudo-ductile laminates on their notch sensitivity and compare the open-hole performance of two different layups. The damage within the laminates was studied using Digital Image Correlation (DIC) during testing and X-ray CT-scan techniques for post-failure analysis. The factors that govern open-hole performance are also discussed.

2. Methods/experimental testing

As mentioned in the work of Javalvand et al. [22], in a pseudo-ductile thin ply glass-carbon hybrid QI laminate, notch sensitivity is expected to decrease with increasing ratio of pseudo-ductile strain to "yield" strain (termed strain ratio) and it can potentially be eliminated when the strain ratio is greater than 3. The definition of pseudo-ductile strain, the "yield" strain and other key measures used in pseudo-ductile laminates are presented in Fig. 1.

Inspired by this, in the current paper, two different pseudo-ductile thin ply angle-ply laminate configurations are presented: one is a laminate with a strain ratio higher than 3 and the other one has a low strain ratio for a contrasting study. The design of the unnotched specimens follows an analytical method developed by Fuller et al. [7].

2.1. Design concepts for unnotched specimen

The criteria used in the design of a pseudo-ductile $[\pm\theta_m/0_n]_s$ laminate follow the analytical method presented by Fuller et al. [7] and is briefly summarised here. Two types of design considerations are made in order to promote the failure in a pseudo-ductile manner:

(1) Once the fibre failure strain of the 0° plies has been reached, the central 0° plies start to fracture and ± θ° plies have to be sufficiently strong to withstand the increased stress at the tip of the crack through the thickness of the adjacent 0° plies (σ_{crack}) to avoid angle-ply failure and ensure the multiple fractures in the central 0° plies (termed fragmentation) that leads to gradual failure. σ_{crack} is calculated as:

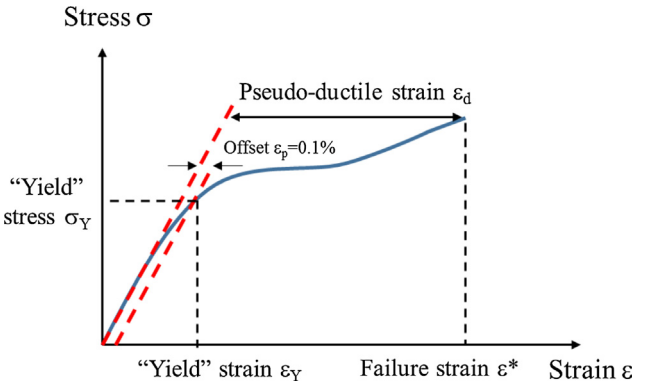

Fig. 1. Definition of pseudo-ductile strain and other key parameters. (For interpretation of the references to colour in this figure legend, the reader is referred to the web version of this article.)

$$\sigma_{crack} = K_t \sigma_x \left(\frac{t}{t_{AP}}\right) \quad (1)$$

where σ_x is the laminate applied stress, t_{AP} is the thickness of angle plies, t is the total laminate thickness and K_t is an assumed stress concentration factor (SCF). An approximate value of 1.08 predicted from a finite element analysis, was used for all of the laminates [11].

(2) The stress concentration at the crack tip promotes a Mode-II delamination at the 0/θ interface. The second design criterion is to assess the delamination stress, ensuring it is higher than the fragmentation stress to avoid the complete delamination of the specimen after the first fracture. The delamination stress σ_{del} is governed by:

$$\sigma_{del} = \frac{1}{t_{AP} + t_{UD}} \sqrt{\frac{2G_{IIc}E_x^{AP}t_{AP}(E_x^{AP}t_{AP} + E_{11}t_{UD})}{E_{11}t_{UD}}} \quad (2)$$

In this equation, G_{IIc} denotes the critical Model II fracture energy, subscripts "UD" and "AP" denote the properties of the 0° plies and angle plies respectively, and E_x^{AP} and E_{11} represent the stiffness of the angle plies and 0° plies respectively.

To achieve the required strain ratio, two approaches can be used, either by increasing the final failure strain or reducing the "yield" strain. Standard modulus fibres normally have a relatively high fracture strain, for example 1.6% for the T300 carbon fibre [23], and a high failure strain of 6% is required for the laminate, which is difficult to achieve in angle-ply laminates whilst retaining good strength and stiffness. Therefore, high modulus fibre prepreg has been used to replace the standard modulus fibre prepreg in the central 0° plies, since the high modulus fibres have a lower fracture strain, for example 0.5% for the TORAYCA YSH70A carbon fibre [24]. Finally, two different laminates were selected in the present study: SM-SM $[\pm 26_5/0]_s$ laminate, where "SM" stands for standard modulus fibre prepreg, and IM-HM $[\pm 25_2/0]_s$, where IM and HM denote intermediate and high modulus fibre prepreg respectively. The SM-SM laminate was based on a similar configuration presented in [7]. In the IM-HM laminate, since the central 0° plies were replaced by high modulus fibre prepreg, the angle plies were adjusted to ± 25° to ensure that they would be strong enough to carry the stress redistribution after the fracture in the 0° plies.

2.2. Materials and laminate specifications

The materials used in each of the tests are commercially available

Table 1
Fibre properties of prepregs.

Fibre Type	Elastic modulus (GPa)	Tensile strain to failure (%)	Tensile strength (MPa)
TORAYCA T300 (Standard modulus) [23]	230	1.6	3530
Mitsubishi Rayon MR60 (Intermediate modulus) [29]	290	2.0	5680
TORAYCA YSH70A (High modulus) [24]	720	0.5	3630

spread tow carbon fibre prepregs including Skyflex USN020A (termed SM) with TORAYCA T300 standard modulus carbon fibre, Skyflex UIN020A (termed IM) with Mitsubishi Rayon MR60 intermediate modulus fibre (both from SK Chemical), and YSH-70A-ThinPreg120EPHTg-402 with ultra-high modulus fibre from North Thin-ply Technology (termed HM). The first two prepregs from SK Chemicals used K50 semi-toughened low-temperature cure resin and the high modulus fibre prepreg from North Thin-ply technology uses a 120 EPHTg-402 type epoxy resin. The elastic properties for the different fibre types and cured laminates are given in Tables 1 and 2 respectively. The SM-SM laminate was laid up from Skyflex USN020A prepreg, cured in the autoclave at 125 °C, as recommended by the manufacturer. The IM-HM laminate was manufactured from Skyflex UIN020A and the North YSH70A prepregs. The curing temperature for the combined laminate was 125 °C, since both prepregs contain resin systems with similar curing temperature. The two prepregs were found to have good compatibility. The degree of curing was examined by using Differential Scanning Calorimetry (DSC) that showed the material had successfully cured. The cured IM-HM laminate was examined using microscope and no phase separation/delamination was observed.

2.3. Specimen design

The unnotched specimens for the SM-SM $[\pm 26_5/0]_s$ and IM-HM $[\pm 25_2/0]_s$ laminates were designed according to the ASTM 3039 standard [25], which stipulates a parallel edge specimen of gauge length 150 mm and width 15 mm. For the open-hole specimens, since the expected damage mechanism for reducing notch sensitivity in these pseudo-ductile laminates is different from conventional laminates, in this initial study to understand the damage mechanism, a single central drilled hole with a diameter of 3.175 mm was used, with a width-to-diameter ratio of 5 and length-to-diameter ratio of 20, giving a specimen width of 16 mm and gauge length of 64 mm. The thicknesses of SM-SM and IM-HM laminates are 0.48 mm and 0.25 mm respectively, which are too thin for testing in open-hole tension due to the compression in the upper and lower edge of the hole that may cause undesired failure. Therefore, the layups of SM-SM $[\pm 26_5/0]_{s2}$ and IM-HM $[\pm 25_2/0]_{s4}$ were used for open-hole specimens, both with similar total thicknesses of about 1 mm. In both cases, glass fibre-epoxy end-tabs of length 40 mm were attached at each end of the specimen. The details of specimen dimensions are specified in Fig. 2.

2.4. Testing setup and equipment

The unnotched and open-hole specimens were tested using an Instron hydraulically-actuated system with a 25 kN load cell, at loading rates of 2 mm/min and 1 mm/min respectively to give similar strain rates on the different length specimens. In both tests, the overall strain was measured by an Imetrum Video Extensometer. The overall longitudinal strain measurements were recorded by tracking targets which were set up near the top and bottom of the gauge length (the targets are shown as orange crosses in Fig. 2).

The Digital Image Correlation (DIC) technique was also employed to evaluate the surface strain field local to the notch and assess any damage development in the open-hole specimen during loading [26,27]. The DIC measurement specifications are summarised in Table 3. It is also worth noting that the imaging apparatus for the SM-SM laminates was set-up to be able to cover the whole specimen area. To perform the DIC measurement on the IM-HM specimens, once it was ascertained that the non-uniform strain field was only in a small region around the open hole, the field of view was reduced to increase spatial and strain resolution.

3. Experimental results and discussion of the unnotched tensile test

3.1. SM-SM $[\pm 26_5/0]_s$ laminates

Fig. 3 shows the stress-strain behaviour of the SM-SM $[\pm 26_5/0]_s$ laminates and the mean values of the key mechanical properties are summarised in Table 4. All five specimens showed consistent pseudo-ductile stress-strain behaviour. In the initial stage of loading, the stress increased approximately linearly with strain. When the specimen was loaded beyond the fibre fracture strain of the T300 fibre (ε_x = 1.6%), an approximately constant stress plateau was observed. During this stage, the fibres in the central 0° plies fragmented progressively and dispersed delamination occurred [7]. The last stage of the curve is a small amount of additional loading after saturation of the fragmentation until the mean failure strain of 3% was reached when the angle plies failed. This stress-strain curve is similar to the one presented in [7], using the same layup but a different fibre type TR30. Overall, gradual failure has been successfully achieved in this configuration, with a “yield” stress of 792 MPa and a pseudo-ductile strain of 1.39%.

3.2. IM-HM $[\pm 25_2/0]_s$ laminates

Fig. 4 shows the un-notched tensile stress-strain behaviour of the IM-HM $[\pm 25_2/0]_s$ laminate and the mechanical properties are summarised in Table 4. All five specimens showed consistent favourable pseudo-ductile tensile stress-strain behaviour although slight discrepancies were observed in the failure strain. From the stress-strain

Table 2
Cured ply mechanical properties of UD laminates.

Prepreg type	E_1 (GPa)	E_2 (GPa)	σ_1 (MPa)	G_{12} (GPa)	υ_{12}	ε_1 (%)	t (mm)	v_f (%)
Skyflex USN020A (T300 fibre)	121[a]	5.4[a]	1936[b]	2.76[c]	0.32	1.6 [23]	0.022[c]	52[c]
Skyflex UIN020A[30] (MR60 fibre)	146	6.6	2800	2.97	0.29	1.9	0.028	50
YSH70A/epoxy [30] (YSH70A fibre)	362	6.0	1810	4.00	0.30	0.5	0.032	50

[a] Estimated from rule of mixtures.
[b] Calculated from E_1 and ε_1.
[c] Measured experimentally.

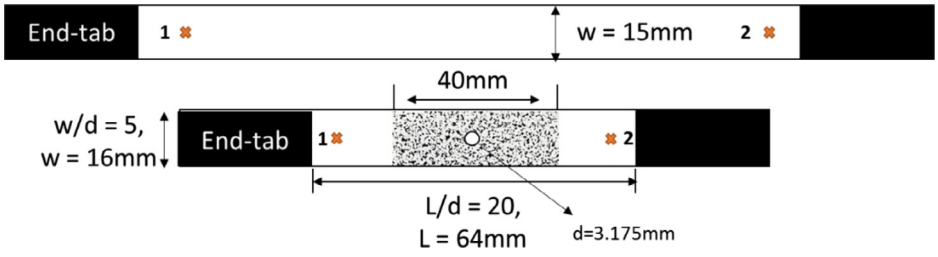

Fig. 2. Schematic of the unnotched and open-hole tensile specimens. Orange crosses on each specimen represent the target points used for tracking longitudinal strain. In the open-hole specimen, the middle region was speckled with black and white dots for surface strain tracking by DIC. (For interpretation of the references to colour in this figure legend, the reader is referred to the web version of this article.)

Table 3
Stereo DIC measurement specifications.

Specimen type	SM-SM $[\pm 26_5/0]_s$	IM-HM $[\pm 25_2/0]_s$
Technique	Stereo DIC	
Software	LaVision DaVis 8.3.1	
Subset size (Pixels)	29	35
Step size (Pixels)	3	3
Camera	VC-Imager 16M	
Lens	Tokina ATX AF 100/2.8	
Resolutions (Pixels)	5065 × 3336	5283 × 3408
Field of view (mm)	101.4 × 66.8	63.0 × 40.6
Spatial resolution (μm)	60	36
Strain resolution (με)	114	68

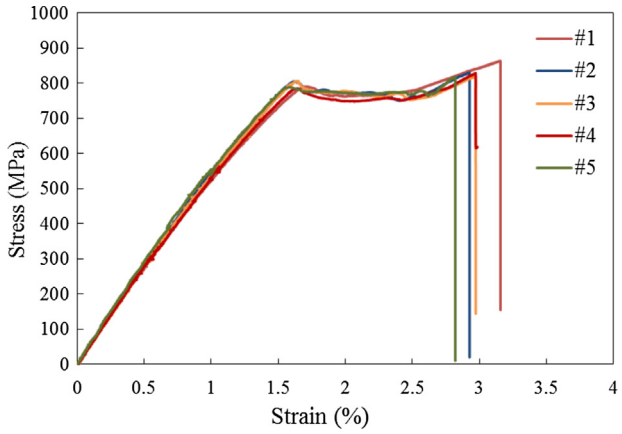

Fig. 3. The unnotched tensile stress-strain behaviour of SM-SM laminates. (For interpretation of the references to colour in this figure legend, the reader is referred to the web version of this article.)

curve, an initial linear response was observed, with an initial modulus of 130 GPa. This modulus is similar to the modulus of a standard modulus fibre prepreg such as Skyflex USN020A prepreg with T300 fibre, and it shows the potential of introducing pseudo-ductile laminates to replace conventional standard modulus carbon fibre laminates. The response was then followed by an approximately constant stress plateau, with multiple small stress variations along the plateau. These stress variations could be due to delamination at the $0/-25$ interface initiating immediately from fragmentation of the high modulus carbon fibre layer [9]. Another possible explanation is the relatively high thickness (t_{UD}/t_{AP}) and modulus (E_{UD}/E_{AP}) of the central 0° plies, which therefore carry a high proportion of the load compared with the angle plies, which can result in a noticeable stress reduction when they

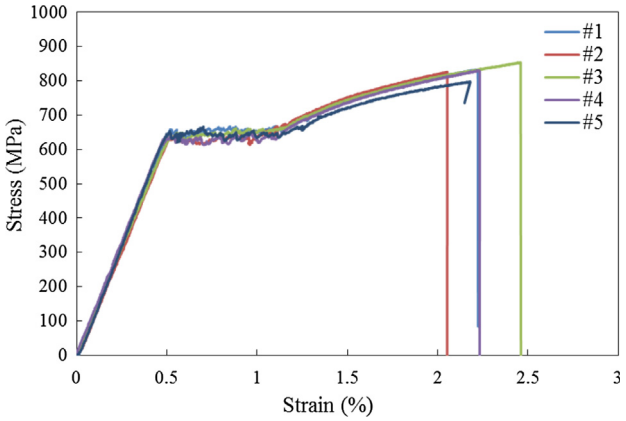

Fig. 4. The unnotched tensile stress-strain behaviour for IM-HM laminates. (For interpretation of the references to colour in this figure legend, the reader is referred to the web version of this article.)

fragment. From the end of the plateau to final failure, the further loading was mainly carried by the angle plies.

The IM-HM $[\pm 25_2/0]_s$ laminate showed pseudo-ductility with a pseudo-ductile strain of 1.54%. Also, it is worth noting that a pseudo-ductile strain to initial strain ratio of 3.02 was achieved. This ratio satisfies the design criterion of obtaining a strain ratio higher than 3 and provides a contrast with the strain ratio of 0.86 for the SM-SM laminate. Although that ratio was based on a quasi-isotropic layup, it was still useful as an initial guideline on the level of pseudo-ductility required.

3.3. Damage analysis via X-ray CT imaging

To understand the damage mechanisms of these two laminates and how the damage developed over the tensile loading, the specimens from both configurations were loaded to various different positions in the stress-strain curve and were analysed using X-ray CT-scanning. All the specimens were immersed in a zinc iodide dye penetrant for at least 24 h and then scanning was performed using a Nikon XTN320 X-ray CT inspection machine. Since a very detailed damage analysis of $[\pm 26_5/0]_s$ laminates with TR30 fibres can be found in previous work [7], only one specimen of SM-SM $[\pm 26_5/0]_s$ is presented in this paper. A detailed characterisation of the IM-HM $[\pm 25_2/0]_s$ laminates is presented in this paper since damage analysis with a similar configuration has not previously been published.

Fig. 5 shows the X-ray image for the SM-SM $[\pm 26_5/0]_s$ specimen taken at the central 0° plies after loading to 1.8% strain, which is 0.2%

Table 4
Mean values for mechanical testing results of SM-SM $[\pm 26_5/0]_s$ and IM-HM $[\pm 25_2/0]_s$ laminates. The coefficient of variation (CV) for each mechanical property are shown in parentheses.

	σ_Y (MPa)	σ^* (MPa)	ε_Y (%)	ε^* (%)	ε_d (%)	$\varepsilon_d/\varepsilon_Y$	E (GPa)
SM-SM $[\pm 26_5/0]_s$	792 (1.1%)	814 (2.1%)	1.62 (1.2%)	3.00 (4.6%)	1.39 (4.6%)	0.86	57 (1.8%)
IM-HM $[\pm 25_2/0]_s$	642 (2.0%)	828 (2.4%)	0.51 (2.0%)	2.22 (6.8%)	1.54 (5.2%)	3.02	130 (3%)

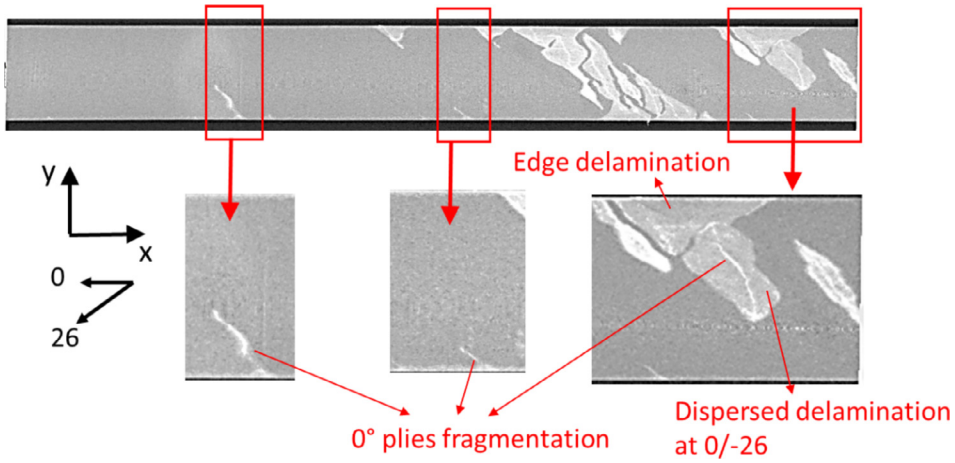

Fig. 5. X-ray images of SM-SM unnotched tensile specimen. (For interpretation of the references to colour in this figure legend, the reader is referred to the web version of this article.)

higher than the nominal fibre fracture strain of the T300 fibre (1.6%) with a scan resolution 0.078 mm. At this strain, fragmentations in the central 0° plies and dispersed delaminations at the 0/-26 interface were expected to have initiated, and the X-ray images show this is the case. Due to the low ply thickness (t = 0.022 mm), interference from surrounding plies occurred, resulting in the captured image at the central 0° layer from CT scanning showing multiple failure modes in varying colour intensities. The fragmentation showed inclined thin white lines, which can be seen propagating from the edge towards to the centre of the specimen. A larger, but less intense white region can be seen around these fragmentations, which is the dispersed delaminations at the 0/−26 interface. It is also worth noting that delamination developed from the free-edge at the −26/26 interface adjacent to the central 0° plies and is shown by a white triangular shape [6]. Some of the edge delaminations joined with dispersed delaminations, forming a larger damaged region.

Fig. 6 shows the X-ray images of the IM-HM $[\pm 25_2/0]_s$ specimens which were loaded to three different strain levels of 0.58%, 1.2% and 2.1% (indicating in Fig. 7). One ultrasonic C-scan image per specimen is also presented to help locate the damage in each specimen, since the X-ray scan was carried on smaller segments along the length of each specimen.

In the X-ray image for 0.58% strain, the inclined thin white lines in the upper region show that fragmentation in the central 0° plies has initiated. Since the strain of 0.58% is close to the fibre fracture strain of

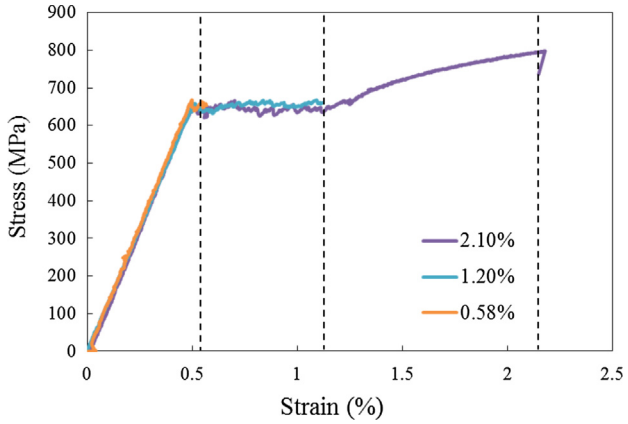

Fig. 7. Stress-strain plot for showing the load/strain level of the IM-HM specimens for X-ray scan. (For interpretation of the references to colour in this figure legend, the reader is referred to the web version of this article.)

0.5%, dispersed delaminations were developed over only a small distance. The images taken of the specimen – halted at a strain of 1.2% – show that the fragmentations were fully saturated along the gauge length and the delamination extended a further distance. Even though some of these inclined strips did not extend fully across the width, these regions were considered to be fragmented, since Fuller et al. [7] showed

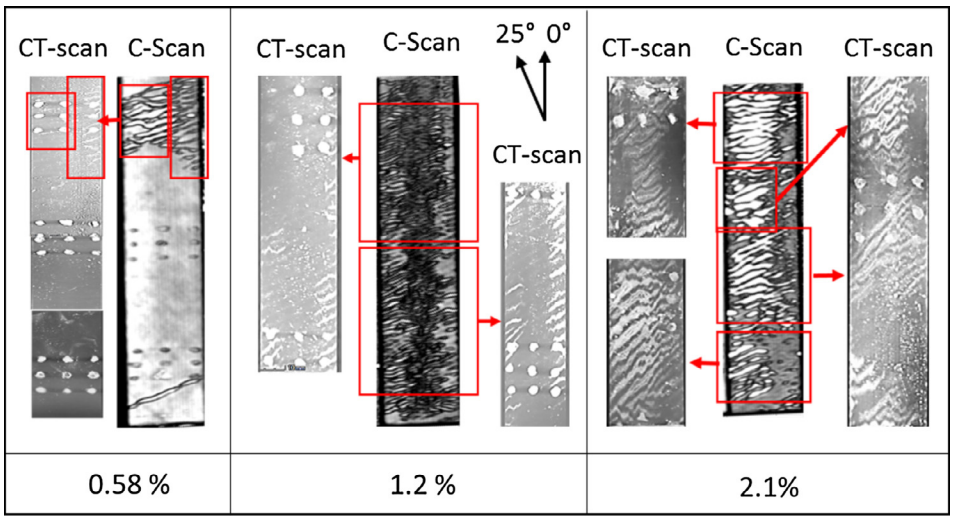

Fig. 6. X-ray images of three IM-HM unnotched tensile specimens loaded to three different levels. C-scan images from the same specimens here are showing the global position of the damage in the specimens. The white dots in each X-ray image are the white paint for video gauge tracking. (For interpretation of the references to colour in this figure legend, the reader is referred to the web version of this article.)

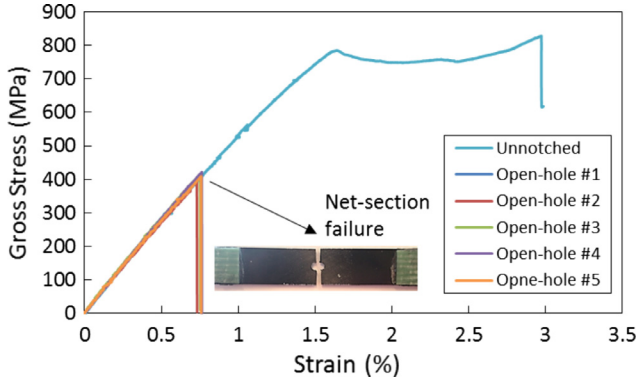

Fig. 8. Stress-strain curves for SM-SM $[\pm 26_5/0]_{s2}$ laminate subjected to open-hole tensile loading. (For interpretation of the references to colour in this figure legend, the reader is referred to the web version of this article.)

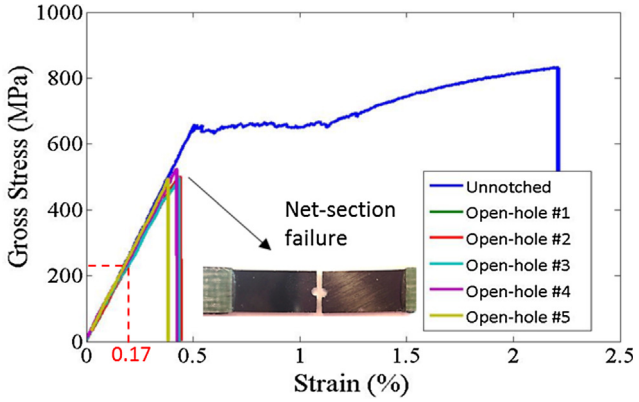

Fig. 9. Stress-strain curves of IM-HM $[\pm 25_2/0]_{s4}$ laminate subjected to open-hole tensile loading. (For interpretation of the references to colour in this figure legend, the reader is referred to the web version of this article.)

that the gap at the fragmentations in the middle could be too small for dye solution to penetrate. When the testing was interrupted at a strain of 2.1%, the dispersed delaminations had propagated extensively and some of the adjacent delaminations were joined together.

Overall, the SM-SM $[\pm 26_5/0]_s$ and IM-HM $[\pm 25_2/0]_s$ laminates both have shown a promising pseudo-ductile stress-strain behaviour, and they gave very different pseudo-ductile strain to "yield" strain ratios of 0.86 and 3.02 respectively. The damage mechanisms of 0° ply fragmentation and dispersed delamination have been observed in both cases.

4. Experimental results and discussion of the open-hole tensile test

4.1. Test results of SM-SM $[\pm 26_5/0]_{s2}$

The open-hole tensile gross section stress is plotted versus the "global" strain measured by the video gauge as shown in Fig. 8, and the unnotched tensile curve of the same laminate is also presented as reference. The averaged mechanical properties have been summarised in Table 5. All five specimens exhibited a similar response: approximately linear up to ultimate net-section failure at the hole. From the previous analysis of unnotched specimens, the X-ray images show that at the end of the stress plateau, full fragmentation in the 0° plies and local dispersed delamination has occurred, which means that any further loading was primarily carried by the angle plies. As a result, in the open-hole tensile loading, once the ligament section has reached the end of the stress plateau in the unnotched stress-strain curve, this section is expected to be fully fragmented and the stress is not able to be redistributed any further. In the present paper, the open-hole performance is assessed against the unnotched "yield" stress since pseudo-ductility only occurs along the stress plateau, and also against the ultimate strength for completeness and consistency with previous work. The average net-section ultimate open-hole tensile strength is 516 MPa, which showed a 35% reduction compared to the unnotched "yield" strength – the maximum stress at which the pseudo-ductile laminates can normally be operated, and 37% less when compared to the unnotched ultimate strength. The significant strength reduction and failure mode of this open-hole specimen is similar to those that have been presented in the studies of thin ply laminates under open-hole tension [18]. Since no significant fragmentation has occurred and all other damage mechanisms have been suppressed in the thin ply laminates prior to failure, the lack of subcritical damage for blunting the stress concentration resulted in a large strength reduction and brittle failure.

4.2. Test results of IM-HM $[\pm 25_2/0]_{s4}$

The open-hole tensile gross stress-strain curves for all five IM-HM specimens are presented in Fig. 9 and averages of key mechanical properties are tabulated in Table 5. All five specimens exhibited a similar linear response in the initial stage, and then a small amount of non-linearity was shown when a strain of 0.17% was reached. This is due to the stress concentrations in the area around the hole – the fragmentation strain of the 0° plies was reached here. In this laminate, an average net-section strength of 627 MPa was achieved, which reached 97% of the unnotched "yield" strength of 642 MPa of the same laminate. If compared to the unnotched ultimate strength of the same laminate, the strength reduction increased to 24%.However, it still can be seen that a higher open-hole strength was retained in the IM-HM laminate than in the SM-SM laminate. This is due to the higher strain ratio in IM-HM laminate than SM-SM laminate. When the strain ratio is sufficiently large, the subcritical damage of 0° ply fragmentation and dispersed delamination can develop to blunt the stress concentration in the IM-HM laminate. Similar to the failed specimen of the SM-SM laminate presented in Fig. 8, the IM-HM specimen separated into two halves across the width through the hole and also shows a clean fracture surface. The fragmentation and localised dispersed delamination damage is within the laminate and cannot be observed visually.

4.3. Damage analysis via digital image correlation

As seen from the open-hole stress-strain behaviour of the two

Table 5
Average test results for open-hole testing of SM-SM $[\pm 26_5/0]_{s2}$ and IM-HM $[\pm 25_2/0]_{s4}$ laminates. The gross strength σ_{gross} was calculated from the full width and net-section strength $\sigma_{net\text{-}section}$ was calculated from a reduced width across the hole. $\sigma_{net\text{-}section}$ is used as the critical strength in this study.

	Unnotched		Open-hole					
	σ_{yield} (MPa)	$\sigma_{ultimate}$ (MPa)	σ_{gross} (MPa)	$\sigma_{net\text{-}section}$ (MPa)	$\varepsilon_{failure}$ [a] (%)	E (GPa)	$\sigma_{net\text{-}section}/\sigma_{yield}$	$\sigma_{net\text{-}section}/\sigma_{ultimate}$
SM-SM $[\pm 26_5/0]_{s2}$	792 (1.1%)	814 (2.1%)	413 4.8%)	516 (4.8%)	0.76 5.3%)	56 (5.4%)	0.65	0.63
IM-HM $[\pm 25_2/0]_{s4}$	642 (2.0%)	828 (2.4%)	502 (2.4%)	627 (2.3%)	0.42 (7.1%)	122 (3.3%)	0.97	0.76

[a] Overall longitudinal strain at failure measured by Video Extensometer.

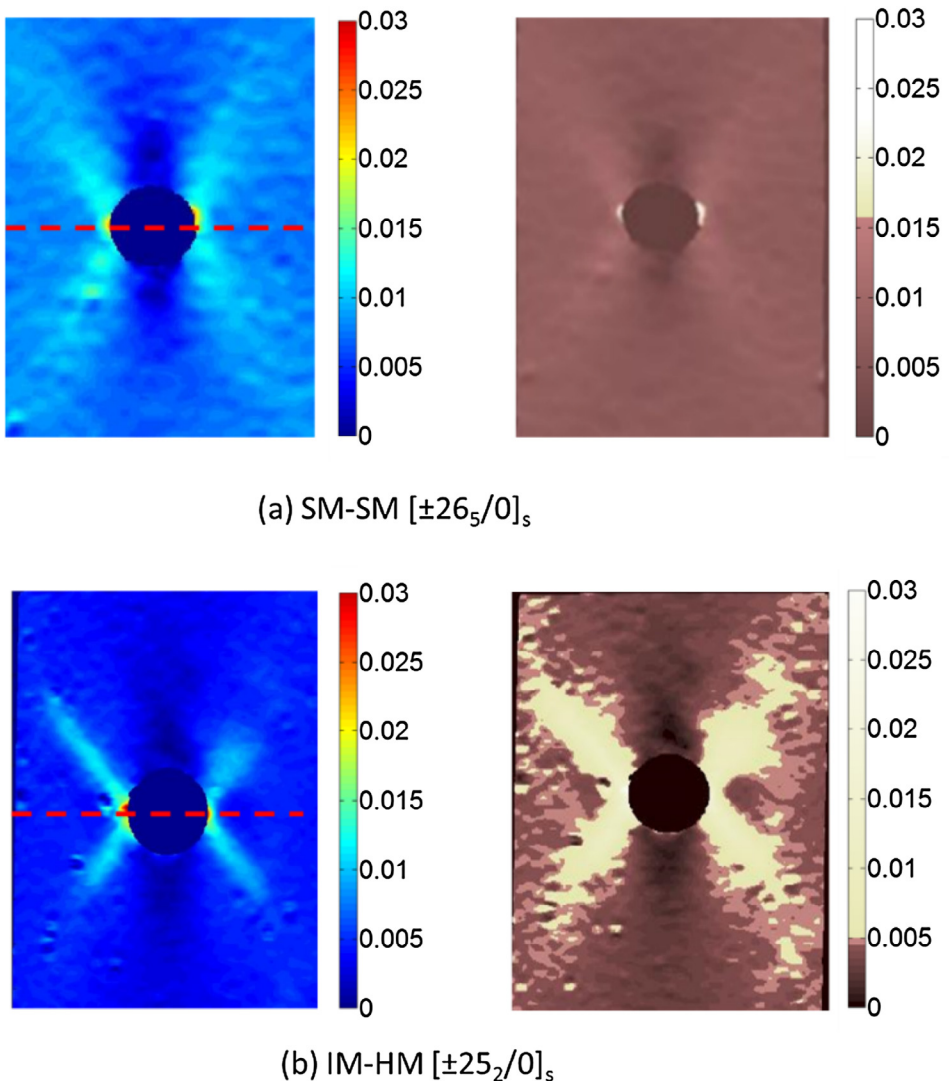

Fig. 10. Original and scaled longitudinal surface strain map of (a) SM-SM $[\pm 26_5/0]_{s2}$ laminate and (b) IM-HM $[\pm 25_2/0]_{s4}$ laminate. All images were taken at 98% of the ultimate strength. (For interpretation of the references to colour in this figure legend, the reader is referred to the web version of this article.)

different laminates in Figs. 8 and 9, the stress concentration has been sufficiently reduced in the IM-HM $[\pm 25_2/0]_{s4}$ laminates to reduce notch sensitivity, but not in the SM-SM $[\pm 26_5/0]_{s2}$ laminates. To further understand the damage mechanisms causing the different notched performance in these laminates and the damage developed during the loading, tracking of the surface strain distribution using the DIC technique was employed. Although DIC is not able to show the damage directly, it can be a useful tool for preliminary analysis of these pseudo-ductile laminates under open-hole tension and for comparing these two different configurations [26].

A surface longitudinal strain field taken at 98% of the failure load of the SM-SM and IM-HM open-hole tensile specimens is plotted in Fig. 10. The surface strain images on the left hand side of Fig. 10 were plotted in a colour map, and the strains in both images can be seen highly concentrated next to the hole edge. However, it is hard to tell any difference between them as the images are shown with the same colour contours. If the fibre fracture strain of the central 0° plies is used as a relative point – the surface strains higher than the fibre fracture strain (1.6% for SM-SM laminate and 0.5% for IM-HM laminate) are plotted in white, whilst the remaining parts are plotted dark. The surface strain distribution was then plotted in the two images on the right hand side of Fig. 10 and these images are called "strain damage maps" in the following paragraphs. As discussed in the damage analysis of the unnotched specimen, fibre fragmentation in the central 0° plies is the first damage to occur, so the area in white is likely to be fragmented.

In the "strain damage map" of the SM-SM laminates, the fragmentation strain has been reached only in the area close to the hole edge. However, in the IM-HM laminates, the white areas extend from the hole boundary approximately parallel to the direction of angle plies, indicating the appearance of fibre fragmentation in the central 0° plies and possibly also some dispersed delaminations at the $0/-25$ interface.

It can be clearly seen that more damage is present in the IM-HM laminates than the SM-SM laminate at 98% of ultimate load, and this damage relieved the stress concentration at the hole edge. Further understanding of how the damage developed during the loading can be gained through several surface strain maps taken at different positions along the stress-strain curves and a local strain versus applied load relation, taken at the critical location of the hole edge.

Figs. 11 and 12 show the "strain damage maps" of the SM-SM $[\pm 26_5/0]_{s2}$ and IM-HM $[\pm 25_2/0]_{s4}$ laminates respectively. For the SM-SM laminate, no damage could be seen until the applied stress reached 373 MPa, 90% of the ultimate stress. After that, the damage only extended to a slightly larger region before ultimate failure. In the "strain damage maps" of the IM-HM specimen, early fibre fragmentation can been observed when the applied stress is 284 MPa, 44% of the open-hole ultimate strength and at a corresponding laminate strain

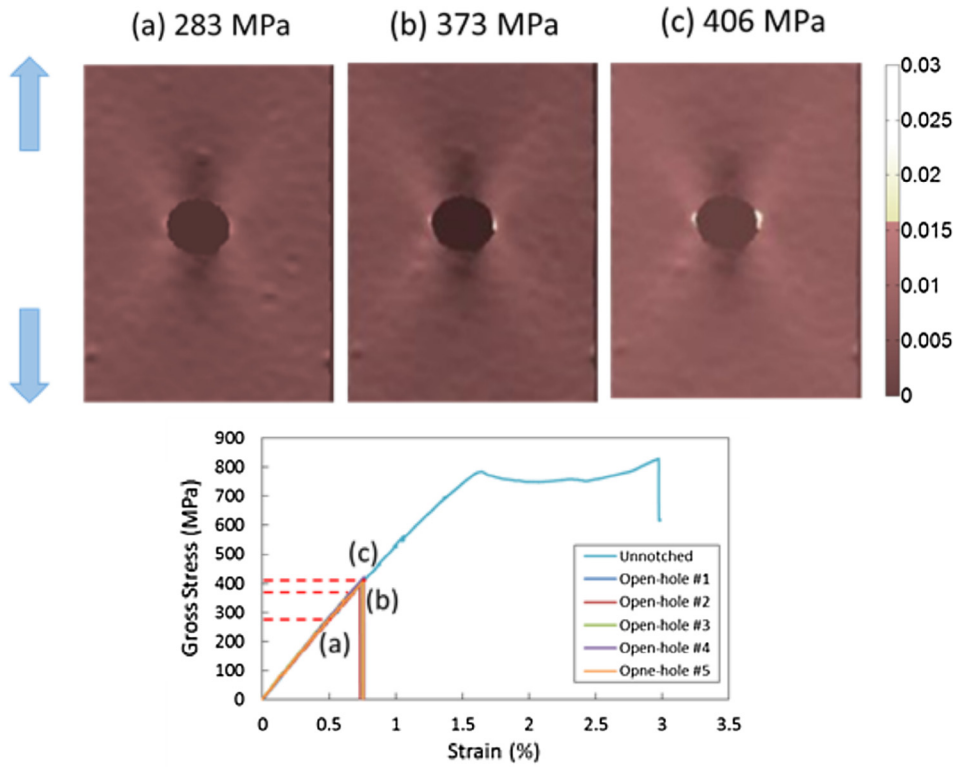

Fig. 11. Scaled longitudinal surface strain maps for SM-SM $[\pm 26_5/0]_{s2}$ laminate at various applied stresses. (For interpretation of the references to colour in this figure legend, the reader is referred to the web version of this article.)

about 0.17%. Consequently, a small amount of nonlinearity has been shown in the gross stress–strain curve starting from this stress.

From Figs. 11 and 12, the hole edge was shown as the first region that has been damaged, therefore the local strain against load curves at the hole edge were plotted in Fig. 13(a) and (b). The hole edge strain of the SM-SM specimen increases approximately linearly with the applied load and only at 98% of ultimate load is there an increase in the slope. By contrast, the IM-HM laminates present a more complicated three-stage local strain variation in Fig. 13(b). The first sharp increase in slope occurred when the specimen was loaded to 46% of ultimate load. At this load, the corresponding strain is 0.5%, the same as the YSH-70A fibre fracture strain. It means the fragmentation initiated in the central 0° plies and resulted in a local stiffness loss. The second critical point in terms of the slope change happened at 94% of ultimate load. At this point, the area around the hole was already close to its unnotched ultimate failure strain and the hole edge was fully damaged in the 0° plies

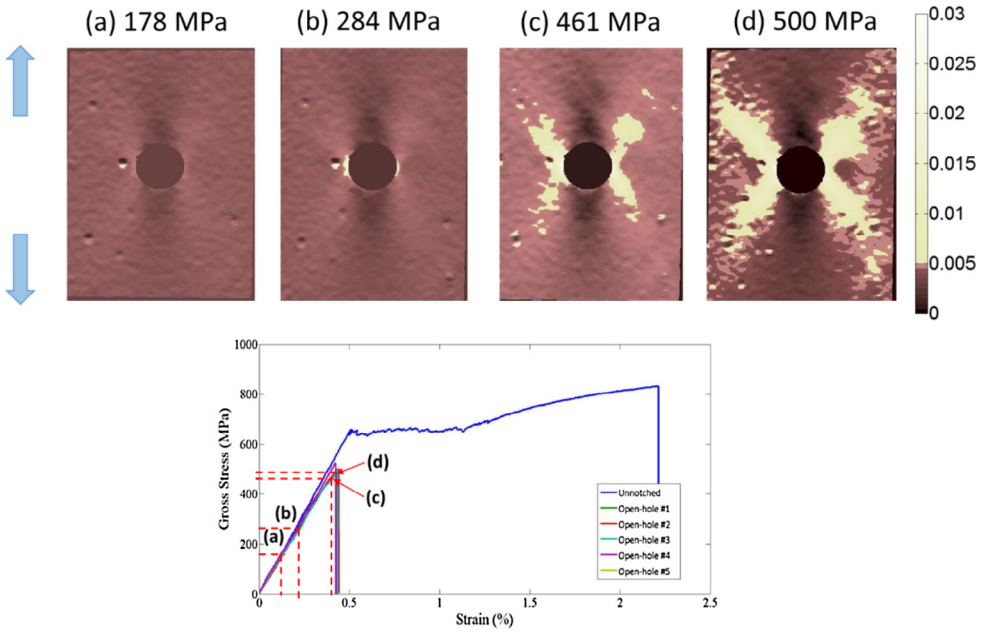

Fig. 12. Scaled longitudinal surface strain maps for IM-HM $[\pm 25_2/0]_{s4}$ laminate at various applied stresses. (For interpretation of the references to colour in this figure legend, the reader is referred to the web version of this article.)

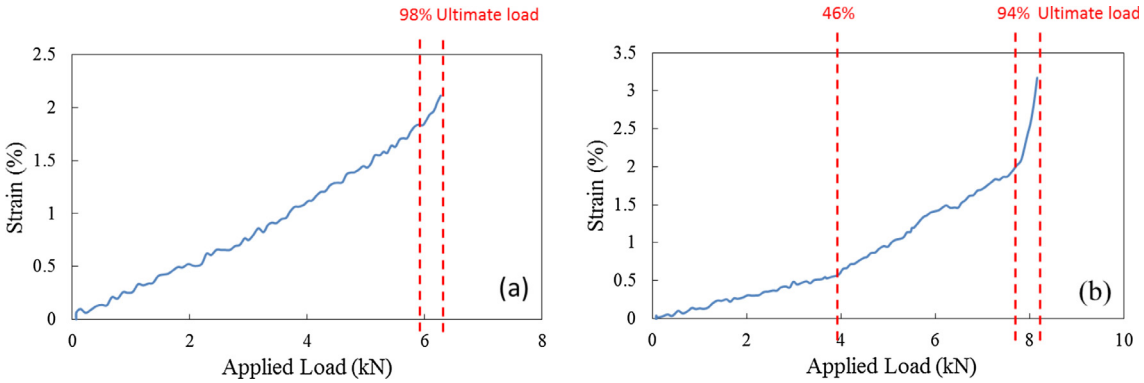

Fig. 13. The strain at the critical point variation with the applied load of (a) the SM-SM laminate and (b) the IM-HM laminate. (For interpretation of the references to colour in this figure legend, the reader is referred to the web version of this article.)

and in the $0/-25$ interface. The angle plies carried most of the load and the entire laminate fractured once the strength of the angle plies was reached.

4.4. Damage analysis: X-ray CT imaging

Even though the surface strain map taken by the DIC technique can identify possible damage within the laminate during loading and explain the differences between the two configurations, it is not a direct technique to observe damage in the laminates. To investigate the damage that has developed in the open-hole tensile loading more accurately, one specimen from each configuration has been loaded to 90% of the mean open-hole ultimate strength, submerged in a zinc iodide dye penetrant solution and then analysed using X-ray CT scans. The X-ray images of the SM-SM and the IM-HM laminate are presented in Figs. 14 and 15 respectively. All damage has been highlighted as a white colour and the grey areas correspond to undamaged material, as discussed in the unnotched tensile testing. The corresponding DIC images from the same specimen at the same load level are also included.

Fig. 14 shows the X-ray images for the SM-SM specimen taken at two different locations of the $0/-\theta$ interfaces through the thickness, illustrated by a red dashed line. The scan resolution is 0.0376 mm. In both images, no critical damage can be observed. The only area highlighted in white is the small region around the hole, which may be machining damage and need not be taken into account [28]. These X-ray images are similar to the X-ray images for open-hole thin ply QI laminates [18,20] – no visible damage at the hole edge or free-edge due to the damage suppression in thin ply laminates. This indicates that the damage mechanisms observed in the unnotched pseudo-ductile laminates have not occurred in the open-hole specimen with the same layup, due to the insufficient strain ratio margin. The "strain damage map" taken at the same load level for the same specimen is shown in Fig. 14(c). No damage is visible, which correlates well with the X-ray images.

Fig. 15(a–d) presents the X-ray images of the IM-HM laminates captured at four different $0/-25$ interfaces through the thickness with scan resolution of 0.044 mm. The DIC "strain damage map" taken at the same loading (90% of ultimate load) is given in Fig. 15(e), showing that fragmentation of the central 0° plies has initiated. The X-ray images show a similar pattern of damage located on both sides of the hole edge and roughly parallel to the $-25°$ direction. The white strips shown in the red bounded boxes have a certain width and are not exactly straight, corresponding to the central 0° plies fragmentation and dispersed delamination associated with fragmentation. This is totally different from the micro-cracks/splitting in angle plies or 0° plies that has been observed in most open-hole testing of laminates.

The X-ray images confirmed that the higher open-hole strength in the IM-HM laminates compared with the SM-SM laminates is due to the damage around the hole initiated by 0° ply fragmentation and dispersed delamination reducing the stress concentration. 0° ply splitting, the main mechanism for blunting the stress concentration in laminates made from conventional thickness plies, was not seen in these pseudo-ductile laminates. The hole size effect observed in conventional laminates is not expected to be the same in this case and it is worth experimental investigation in future work. It is also shown that the DIC

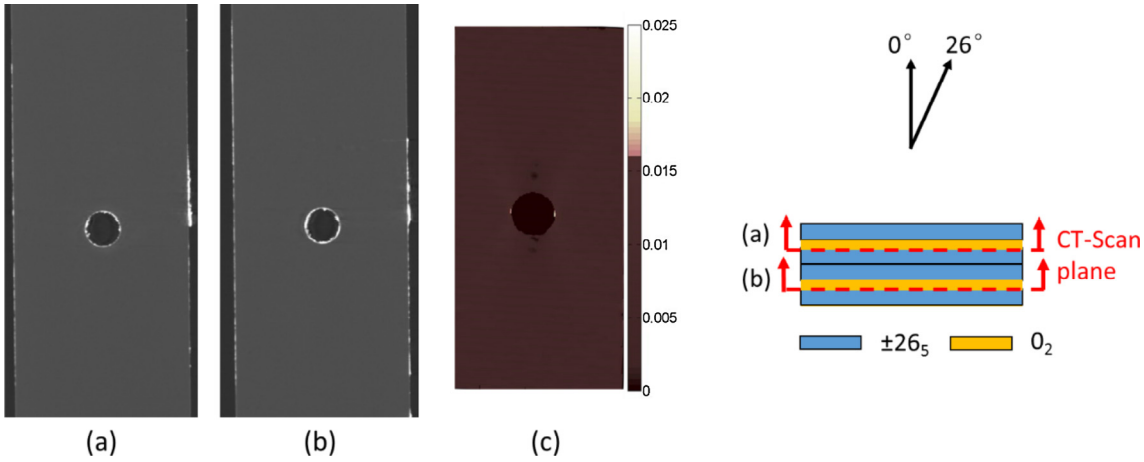

Fig. 14. (a) (b) X-ray images for the open-hole SM-SM $[\pm 26_5/0]_{s2}$ laminate, taken at two different $0/-26$ interfaces shown as the red dashed line. (c) The "strain damage map" of the same specimen at the same load (90% of ultimate load). (For interpretation of the references to colour in this figure legend, the reader is referred to the web version of this article.)

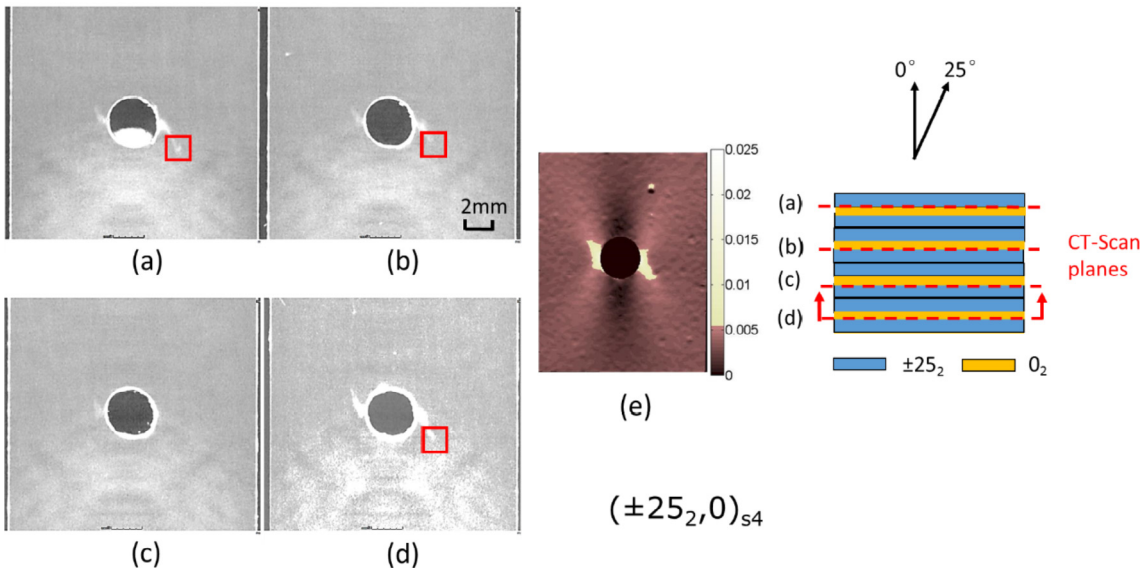

Fig. 15. X-ray images for the open-hole IM-HM $[\pm 25_2/0]_{s4}$ laminate, taken at four different $-25/0$ interface shown in the red dashed line from (a) to (d). It should be noted that the large white region at the bottom of all four images and the white "ellipse" in the hole in (a) are the rubber used to hold the specimen during CT scan, so do not constitute any damage. (e) "Strain damage map" predicted from DIC in the same specimen at the same load level (90% of ultimate load). (For interpretation of the references to colour in this figure legend, the reader is referred to the web version of this article.)

technique is a sufficient tool to determine where the damage is likely to have occurred and for a preliminary verification of what the possible damage mechanisms are in the pseudo-ductile thin ply angle-ply laminates under open-hole loading.

5. Conclusions

Pseudo-ductile tensile stress-strain behaviour has been demonstrated in unnotched SM-SM $[\pm 26_5/0]_s$ and IM-HM $[\pm 25_2/0]_s$ laminates. The ratio of pseudo-ductile strain to "yield" strain for the SM-SM laminate and IM-HM laminate were 0.86 and 3.02 respectively. Central 0° ply fragmentation and dispersed delaminations have been shown as the main damage mechanisms in both tested laminates via X-ray CT scanning. However, their performance was different in the presence of stress concentrations when they were subjected to open-hole tensile loading: the SM-SM laminate is sensitive to the stress concentrations, but the notch sensitivity in IM-HM laminate is reduced. The open-hole net-section strength is similar to the unnotched "yield" strength of these laminates and less strength reduction is observed in the IM-HM laminate than the SM-SM laminate, when comparing the notched strength to the unnotched ultimate strength.

The X-ray images showed a larger damaged area in the IM-HM specimen than in the SM-SM at 90% of ultimate loading. The damage mechanisms of unnotched IM-HM laminates, with 0° ply fragmentation and dispersed delamination, have also been seen in the open-hole specimens with the same layup. These damage mechanisms relieved the stress concentration around the hole in the IM-HM laminate, resulting in an enhanced notched strength and reduced notch-sensitivity of the IM-HM laminates compared with the SM-SM laminates. The main governing factor for notch-sensitivity was identified as the ratio of pseudo-ductile strain to "yield" strain. If the strain ratio is low, the strain at the hole edge reaches the unnotched tensile failure strain, whilst the rest of the region is still below the fibre fragmentation strain and damage progression and associated stress redistribution is limited in the laminate. But if the strain ratio is high, full load redistribution can take place.

Digital image correlation has been found to be a useful tool to identify damage development in pseudo-ductile thin ply angle-ply laminates with central 0° plies. From the surface longitudinal strain distribution and the local strain variation around the hole, the initial damage in the open-hole SM-SM specimens was found to occur at 98% of the ultimate load. However, damage was found in the IM-HM specimen when the specimen was loaded to only 46% of its ultimate load. The presence of damage at an early stage relieved the stress concentration by the damage developed within the laminates.

From the study of both laminates presented above, it has been successfully demonstrated that the notch-sensitivity can be reduced in thin ply laminates by taking advantage of the damage mechanisms of pseudo-ductile thin ply angle-ply laminates with central 0° plies. By proper selection of materials and layup in these laminates, an optimised configuration can be provided to achieve the full potential in both unnotched and notched applications.

Acknowledgements

This work was funded by the ACCIS Centre for Doctoral Training in Advanced Composites (grant number EP/G036772/1) and under the UK Engineering and Physical Sciences Research Council (EPSRC) Programme Grant EP/I02946X/1 on High Performance Ductile Composite Technology in collaboration with Imperial College, London. The underlying data to support the conclusions are provided within this paper.

References

[1] Boncel S, Sundaram RM, Windle AH, Koziol KKK. Enhancement of the mechanical properties of directly spun CNT fibers by chemical treatment. ACS Nano 2011;5:9339–44.
[2] Allaer K, De Baere I, Lava P, Van Paepegem W, Degrieck J. On the in-plane mechanical properties of stainless steel fibre reinforced ductile composites. Compos Sci Technol 2014;100:34–43.
[3] Callens MG, Gorbatikh L, Verpoest I. Ductile steel fibre composites with brittle and ductile matrices. Compos Part A Appl Sci Manuf 2014;61:235–44.
[4] Swolfs Y, Crauwels L, Gorbatikh L, Verpoest I. The influence of weave architecture on the mechanical properties of self-reinforced polypropylene. Compos Part A Appl Sci Manuf 2013;53:129–36.
[5] Fuller JD, Wisnom MR. Exploration of the potential for pseudo-ductility in thin ply CFRP angle-ply laminates via an analytical method. Compos Sci Technol 2015;112:8–15.
[6] Fuller J, Wisnom M. Pseudo-ductility and damage suppression of thin ply CFRP angle-ply laminates. Compos Part A Appl Sci Manuf 2015;69:64–71.
[7] Fuller JD, Jalalvand M, Wisnom MR. Combining fibre rotation and fragmentation to achieve pseudo-ductile CFRP laminates. Compos Struct 2016;142:155–66.
[8] Pimenta S, Robinson P. Wavy-ply sandwich with composite skins and crushable core

for ductility and energy absorption. Compos Struct 2014;116:364–76.
[9] Czél G, Jalalvand M, Wisnom MR. Design and characterisation of advanced pseudo-ductile unidirectional thin-ply carbon/epoxy-glass/epoxy hybrid composites. Compos Struct 2016;143:362–70.
[10] Czél G, Wisnom MR. Demonstration of pseudo-ductility in high performance glass/epoxy composites by hybridisation with thin-ply carbon prepreg. Compos Part A Appl Sci Manuf 2013;52:23–30.
[11] Jalalvand M, Czél G, Wisnom MR. Damage analysis of pseudo-ductile thin-ply UD hybrid composites – a new analytical method. Compos Part A Appl Sci Manuf 2015;69:83–93.
[12] Swolfs Y, Meerten Y, Hine P, Ward I, Verpoest I, Gorbatikh L. Introducing ductility in hybrid carbon fibre/self-reinforced composites through control of the damage mechanisms. Compos Struct 2015;131:259–65.
[13] Yu H, Longana ML, Jalalvand M, Wisnom MR, Potter KD. Pseudo-ductility in intermingled carbon/glass hybrid composites with highly aligned discontinuous fibres. Compos Part A Appl Sci Manuf 2015;73:35–44.
[14] Diao H, Bismarck A, Robinson P, Wisnom MR. Pseudo-ductile behaviour of unidirectional fibre reinforced polyamide-12 composite by intra-tow hybridization. In: ECCM16-16th European Conference on Composite Materials, Seville, Spain, 1–8; 2007.
[15] Kortschot MT, Beaumont PWR. Damage mechanics of composite materials: I-measurements of damage and strength. Compos Sci Technol 1990;39:289–301.
[16] Morris CEH, DH. Role of delamination and damage development on the strength of thick notched laminates, delamination and debonding of materials. In: Johnson WS, editor. Am Soc Test Mater ASTM STP 876; 1985. p. 424–447.
[17] Green BG, Wisnom MR, Hallett SR. An experimental investigation into the tensile strength scaling of notched composites. Compos Part A Appl Sci Manuf 2007;38:867–78.
[18] Sihn S, Kim RY, Kawabe K, Tsai SW. Experimental studies of thin-ply laminated composites. Compos Sci Technol 2007;67:996–1008.
[19] Furtado C, Arteiro A, Catalanotti G, Xavier J, Camanho PP. Selective ply-level hybridisation for improved notched response of composite laminates. Compos Struct 2016;145:1–14.
[20] Arteiro A, Catalanotti G, Xavier J, Camanho PP. Notched response of non-crimp fabric thin-ply laminates. Compos Sci Technol 2013;79:97–114.
[21] Amacher R, Cugnoni J, Botsis J, Sorensen L, Smith W, Dransfeld C. Thin ply composites: experimental characterization and modeling of size-effects. Compos Sci Technol 2014;101:121–32.
[22] Jalalvand M, Czél G, Wisnom MR. Reducing the notch sensitivity of quasi-isotropic layups using thin-ply hybrid laminates. In: Proceedings of the 30th Annual Technical Conference of the American Scociety for Composites 2015, East Lansing, Michigan, USA, 28–30th September; 2015.
[23] Torayca. T300 Data Sheet; 2002. p. 6–7.
[24] Nippon Graphite Fiber Corporation. Nippon Granoc Yarn YSH-A Series; 2010. p. 1–2.
[25] ASTM International, West Conshohocken, PA, USA. Standard test method for tensile properties of polymer matrix composite materials, ASTM D3039/D3039M – 08; 2011.
[26] Gill AF, Robinson P, Hitchings D. Measurement of damage progression in open hole tension tests. In: ICCM16 – 16th International Conference on Composite Materials, Tokyo, Japan, 3–7, 2007.
[27] Toubal L, Karama M, Lorrain B. Stress concentration in a circular hole in composite plate. Compos Struct 2005;68:31–6.
[28] Tan SC. Stress concentrations in laminated composites. Lancaster, Pennsylvania, USA: Technomic Publishing Company, Inc; 1994.
[29] Properties TF. PYROFIL TM MR60H 24K; 2008.
[30] Fuller JD, Jalalvand M, Wisnom MR. A pseudo ductile angle-ply sub-laminate approach for multidirectional thin-ply CFRP laminates. In: Proc ECCM-17, 17th Eur Conf Compos Mater 2016: 26–30.